Available online at www.sciencedirect.com

ScienceDirect

Procedia Engineering 110 (2015) 82 – 89

Procedia Engineering

www.elsevier.com/locate/procedia

4th International Conference on Tissue Engineering, ICTE2015

A biomechanical approach for bone regeneration inside scaffolds

Carolina Gorriz[a], Frederico Ribeiro[a], José M. Guedes[a], Paulo R. Fernandes[a]*

[a] *IDMEC, Instituto Superior Técnico, Universidade de Lisboa, Lisboa 1049-001, Portugal*

Abstract

The factors that conduct to an optimal scaffold performance haven't been fully determined and for that reason the scaffolds behavior and action inside the human body continue to be extensively analyzed through experimental and numerical studies. In this work, a computational model is developed in order to concurrently analyze the scaffold biodegradation and bone regeneration. The scaffold is assumed to be a periodic structure made by the repetition of a representative volume element with periodic properties. For a representative volume element a suitable degradation model and a mechano-regulated bone tissue regeneration model are combined to predict the tissue regeneration within the scaffold. The evolution of effective elastic and permeability properties of the periodic media is assessed by an asymptotic homogenization method. Results are in a good agreement with other computational and experimental data, with the most relevant findings being that under normal loading conditions (1 MPa), increasing the scaffold porosity resulted in higher percentages of bone formation, while when comparing scaffolds with ranging porosity values of 50%, 65% and 80%, with an applied load of 2 MPa, a superior bone formation was predicted for the 65% one. This indicates that for higher load magnitudes, the porosity must be balanced with mechanical stability. The developed computational model is a useful tool to provide new insights on the design and behaviour of biodegradable scaffolds.

© 2015 The Authors. Published by Elsevier Ltd. This is an open access article under the CC BY-NC-ND license (http://creativecommons.org/licenses/by-nc-nd/4.0/).

Peer-review under responsibility of IDMEC-IST

Keywords: Bone scaffolds; Biodegradation; Bone Regeneration; Bone substitutes Homogenization

1. Introduction

There are over 15 million fracture cases globally [1] and an estimated 2.2 million bone graft procedures are performed annually to promote fracture healing or to fill defects [2]. Sometimes the common solutions, such as autografts, allografts and implantation of non-biological implants, are not suitable due to the bone limited supply, donor site morbidity, disease transmissions, host immune response, and, for the implants case, failure may occur after

* Corresponding author. Tel.: +351-218417925; fax: +351-218417915.
E-mail address: prfernan@dem.ist.utl.pt

1877-7058 © 2015 The Authors. Published by Elsevier Ltd. This is an open access article under the CC BY-NC-ND license (http://creativecommons.org/licenses/by-nc-nd/4.0/).
Peer-review under responsibility of IDMEC-IST
doi:10.1016/j.proeng.2015.07.013

a certain time, due to the different mechanical properties of the material comparing with the original tissue [2]. Scaffold-based strategies for Bone Tissue Engineering have become more popular in providing an alternative to the previous solutions, combining cells, bioactive molecules and a three-dimensional structural porous matrix in order to create an appropriate substitute that repairs and regenerate the damaged tissue.

The development of scaffolds with optimal performance has motivated the development of computational models for scaffold design [3-5], as well as the development of models to simulate the scaffold degradation and the respective bone formation. Models to predict tissue regeneration inside scaffolds (degradation and bone formation) differ each other on the biodegradation model used [6-9] and on the bone formation approach [10-12].

In line with this research on scaffold design, the main goal of this work is the study of the dynamic and interdependent process of degradation and the cell/tissue invasion in an artificial bone substitute, accomplished through the development of a computational model combining the scaffold degradation and the bone tissue regeneration process. The computational model assumes the scaffold to be a periodic structure constituted by several volume elements with periodic properties, which allow us to study only a representative volume element of the scaffold. The model encompasses three main sections: a degradation model applicable to polymers with a mass degradation profile, comprising the hydrolysis process and its enhancement by autocatalysis; one mechano-regulated bone tissue regeneration model based on cell differentiation and growth theories; and an asymptotic homogenization method that allows the calculation of the effective elastic and permeability properties of the system.

2. Methods

The starting point is to assume the scaffold as a periodic structure obtained by the repetition of a Representative Volume Element (RVE) which has periodic properties. Because of that, the computational model only uses one RVE of the scaffold - a unit cell design model - as object of study. This approach allow us to analyze periodic scaffold obtained through topology optimization [4, 5, 13].

The implemented degradation model was an adaptation of the one proposed in [10]. The domain is divided into a finite number of elements, to which a state is assigned: 1 for hydrolysable states, 0.001 for hydrolyzed ones and 0 for the remaining void states. For every element, a degradation probability is attributed. In every iteration, for every element with state $\chi_H = 1$, a random generated number, r, is compared to that probability. If $P(\lambda_0,t) > r$, the element is hydrolyzed and its state altered to $\chi_h = 0.001$.

$$P(\lambda_0,t) = \frac{\lambda_0 e^{-\lambda_0 t}\left[1+\beta(e^{C_m}-1)\right]}{V_0\, V(t)} \tag{1}$$

where λ_0 is the degradation rate constant without autocatalytic effect, β is a constant to regulate the contribution of autocatalysis, C_m is the concentration of the monomers/byproducts resultant from previous degradation, V(t) is the volume fraction of polymer matrix at time t and V_0 is the initial volume fraction. C_m is a nodal variable increased when an element is degraded, by adding the mass of the degraded chains to all the adjacent nodes, n, of that element:

$$C_{mnew}^{N} = C_m^N + \frac{\chi_H - \chi_h}{n} \tag{2}$$

The monomers motion through the scaffold is described by a diffusion equation, with attribution of different diffusivity constants during the degradation process, according to the element properties.

The implemented bone regeneration model is based on cell differentiation and growth theories, where cellular process such as mitosis, migration, differentiation and apoptosis are mechano-regulated. It is an adaptation of the healing model proposed in [14]. The key players are Mesenchymal Stem Cells (MSCs), fibroblasts, chondrocytes and osteoblasts. The respective cell concentrations are expressed as c_s, c_f, c_c and c_b.

The mechanical stimulus, ψ, is assumed to be dependent on the principal strains, ε_I, ε_{II} and ε_{III}, and on the octahedral strain, ε_{oct}:

$$\psi(x,t) = \sqrt{(\varepsilon_I - \varepsilon_{oct})^2 + (\varepsilon_{II} - \varepsilon_{oct})^2 + (\varepsilon_{III} - \varepsilon_{oct})^2} \tag{3}$$

$$\varepsilon_{oct} = \frac{\varepsilon_I + \varepsilon_{II} + \varepsilon_{III}}{3} \tag{4}$$

The MSCs differentiation is modeled by:

$$f_{differentiation}(\psi, t_m) = \begin{cases} h_{intramembranous}(\psi, t), & \psi_{lim} < \psi < \psi_{bone} \text{ and } t > t_m^b \\ g_{differentiation}(\psi, t), & \psi_{bone} < \psi < \psi_{cartilage} \text{ and } t > t_m^c \\ l_{differentiation}(\psi, t), & \psi_{cartilage} < \psi < \psi_{fibrous} \text{ and } t > t_m^f \\ -c_s, & \psi_{death} < \psi \\ 0, & \text{other cases} \end{cases} \tag{5}$$

where $hi_{intramembranous}$, $g_{differentiation}$ and $l_{differentiation}$ are functions that define the differentiation of MSCs to osteoblasts, chondrocytes and fibroblasts, respectively. Each one is selected according to predefined mechanical stimulus boundaries and according to cell type specific maturation times that must be achieved. The last branch represents MSCs apoptosis caused by high mechanical stimulus.

Besides differentiation, MSCs may also undergo proliferation and migration. Proliferation is described by Equation 6, being only dependent on the stem cells concentration and on the mechanical stimulus, until ψ reaches ψ_{death}, thereafter proliferation is stopped and its value becomes zero. Migration is expressed by Equation 7, modeling the random motion of MSCs.

$$f_{proliferaton}(c_s, \psi) = \frac{\alpha_{proliferaton}\psi}{\psi + \psi_{proliferaton}} c \tag{6}$$

where $\alpha_{proliferation}$ and $\psi_{proliferation}$ are MSCs proliferation constants.

$$f_{migration}(c_s) = -D_0 \nabla^2 c_s, \tag{7}$$

where D_0 is a diffusion coefficient.

Proliferation and migration of other cells are disregarded as their impact is quite small. The appearance of chondrocytes and fibroblasts is made exclusively through the direct transition from MSCs. Bone cells are created from MSCs differentiation, that initially is dependent on the surrounding bone cell concentration, being modeled as a diffusion process, until a vascularization threshold is surpassed, enabling MSCs to differentiate directly into bone cells. Osteoblasts may also be created as the result of cartilage calcification. This phenomenon is modeled as diffusion, dependent on the advance of an ossification front, until an osteoblasts concentration limit is surpassed, when all cartilage cells die and are instantly replaced.

Each cell type produce a different type of Extracellular Matrix (ECM): MSCs produce granulation tissue, chondrocytes produce cartilage, fibroblasts produce fibrous tissue and osteoblasts produce bone. The production rate of ECM volume is dependent on the specific cell concentration and on the matrix production rate per cell type, Qi.

$$\frac{\partial V_{matrix}^i}{\partial t} = c_i \cdot Q_i \tag{8}$$

The mechanical and permeability properties of the scaffold material, here considered to be 50:50 poly(lactic-co-glycolic acid) (PLGA), are presented in Table 1. When tissues are created, the nodal properties are the result of the

combination of different tissues, so they are calculated using an average with the tissues volume fractions. The values used for each tissue are also presented in Table 1.

Table 1. Mechanical and permeability properties of the scaffold material and the different tissues.

	PLGA	Granulation tissue	Bone tissue	Cartilage	Calcified cartilage	Fibrous tissue
E (MPa)	1200[11]	0.2[9]	982.489[10]	27.055[10]	57.055[10]	80.078[10]
ν	0.33[11]	0.167[9]	0.296[10]	0.104[10]	0.108[10]	0.128[10]
k ($\times 10^{-14}\ m^4/Ns$)	0.001[9]	1[9]	0.001[9]	0.5[9]	0.5[9]	1[9]

The effective elastic and permeability properties of the system are calculated using the asymptotic homogenization method, described in [15], through the following equations:

$$D_{ijkl} = \frac{1}{|Y|}\int_Y \left(E_{ijkl} - E_{ijpq}\frac{\partial \chi_p^{kl}}{\partial y_q} \right) dY \tag{9}$$

where $|Y|$ is the volume of the entire unit cell with the void and χ^{kl} represents the characteristic deformations that result from six unit strains applied solely to the unit cell [16].

$$K_{im}^H = \frac{1}{|Y|}\int_Y K_{ij}\left(\delta_{jm} - \frac{\partial \chi^m}{\partial y_j} \right) dY \tag{10}$$

where χ^m describes the microstructure pressure perturbations for a unit average pressure gradient in each direction m [16].

The presented model was programmed in Python™ scripts that accessed the functionality of the commercial software Abaqus®. Afer the geometry is generated, the program enters a cycle, with a one day step. Inside the cycle, a poroelastic analysis is executed for the calculation of the mechanical stimulus, enabling the prediction of MSCs differentiation.

Values of mechanical and permeability properties at every element are printed to text files and read by PREMAT, the finite element implementation in FORTRAN of the homogenization method [16].

Next, the random migration of MSCs and the advance of the ossification front are defined, by performing mass diffusion analyses. Finally, the degradation process is simulated and a new mass diffusion analysis for the released monomers is required.

3. Results and Discussion

The model had two different implementations, in order to perform two and three dimensional analyses. 3D permeability maximized microstructures, obtained by Dias et al. [4] through a topology optimization algorithm, were used as well as their cross-sections. In addition, 2D ones were designed to examine in greater detail the effect of porosity and loading conditions. The unit cells had 1mm in every direction.

The more relevant findings, regarding the 2D analyses, were that, under normal loading conditions (1 MPa), when increasing the scaffold porosity, higher percentages of bone formation were predicted. For the same configuration, a higher porosity translates into a scaffold with a lower effective mechanical stiffness, increasing the mechanical stimulus influencing the cells. At the beginning, since the cell processes are regulated by the mechanical stimulus, the lower porous scaffolds conduct to more MSCs proliferation and differentiation. However, after a delayed period in which the polymer matrix becomes weaker due to the degradation, the higher porosity scaffolds end up producing much more cartilage due to earlier higher mechanical stimulus and, when endochondral ossification starts to occur, the bone formation is intensified. These results are corroborated by similar ones obtained in [17].

When comparing scaffolds with ranging porosity values of 50%, 65% and 80%, with an applied load of 2 MPa, a superior bone formation was predicted for the 65% one. This occurs because lower porosity scaffolds, that have higher mechanical properties, reduce the high stresses acting on the cells. This decrease is beneficial, because a very high mechanical stimulus will not belong to the ranges that lead to tissues formation and, in the limit, may lead to cells death. These findings are in accordance with experiments, since better performances were achieved for scaffolds with porosity values inferior to 70% [18]. It is reasonable to assume that for even higher load magnitudes, lower porosities would have to be adopted, in order to maintain the same performance.

The degradation profiles for all simulations (2D and 3D) were very similar, so as example the results for the 3D microstructure, with 35% porosity, will be presented and discussed. Figure 1 presents the normalized average molecular weight in percentage as a function of time, to allow an analysis of the degradation behavior. Experimental values from the works of Wu and Wang [19] and Oh et al.[20] are included in order to enable a comparison to assess the validity of the implemented degradation model. Both studies presented values of average molecular weight, so normalization was required to enable comparison.

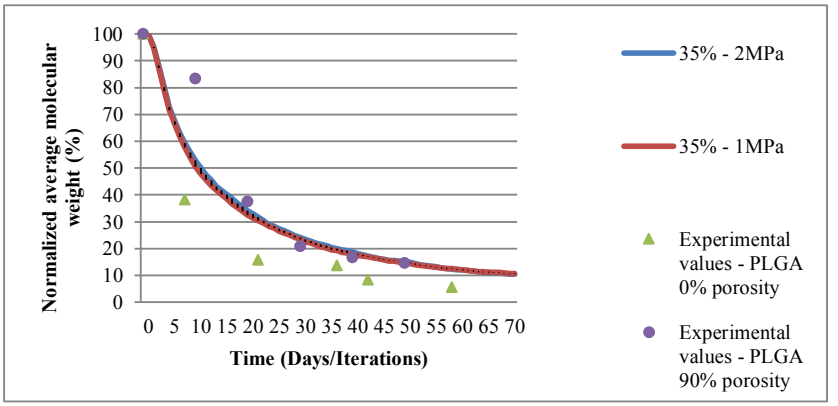

Fig. 1. Comparison between the simulation results and reported experimental results of normalized average molecular weight (%) as a function of time during biodegradation.

The obtained values form a decreasing exponential over the degradation time, indicating a good agreement with what is expected in a bulk degradation, representing a simultaneous degradation on the surface and in the bulk of the material. On the last days, there is a small deceleration compared to what was expected. That could be interpreted as a need to perform a slight adjustment in the degradation rate constant or in autocatalysis factor.

The evolution of tissues formation between all simulations also resembled. By way of illustration some of the 3D results, obtained for the same 35% porosity microstructure, are presented in Figure 2.

On the first days, the main occurrences are the degradation of the polymer matrix and the proliferation and diffusion of the MSCs. Bone is the first tissue to be formed, appearing from the boundaries of the domain in regions located near the scaffold matrix. Around day 16, the areas surrounding the polymer matrix are under the influence of a mechanical stimulus that favors mainly the differentiation into chondrocytes and osteoblasts. About the same time, MSCs differentiation into fibroblasts occurs. Fibrous tissue formation is observed in areas of higher mechanical stimulus.

From this point on, MSCs start migrating more profusely towards the inside of the polymer matrix as the number of voids is ever increasing. Due to the production of new tissues, that possess higher mechanical properties, the mechanical stability of the system is increased, further promoting the formation of bone in those locations.

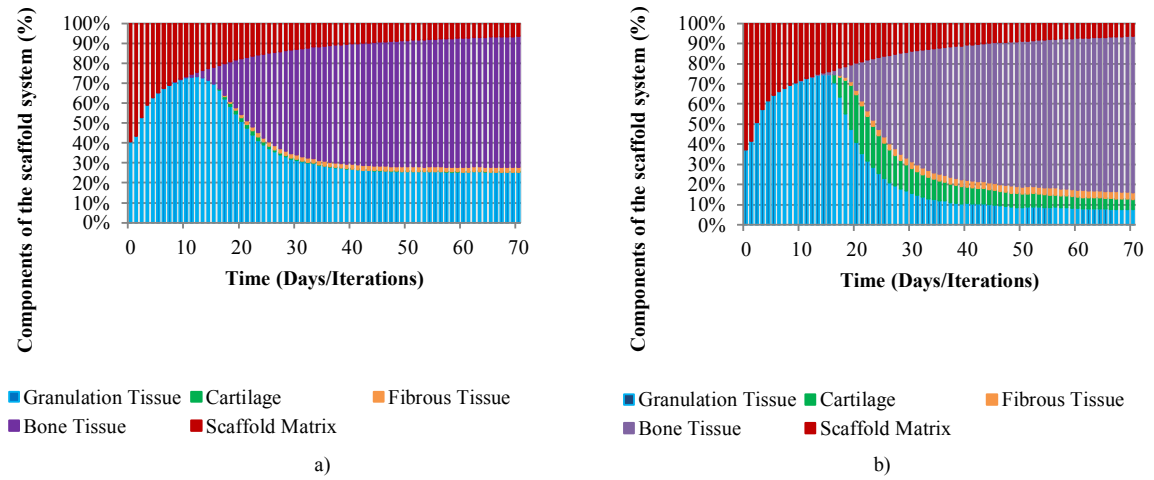

Fig. 2. Percentage of neo-tissue formation as a function of time, for an applied load of (a) 1MPa, and (b) 2MPa.

Around day 22/23, the bone cells, created mainly by intramembranous ossification, invade the matrix composed of calcified cartilage and replace it. After that, and until day 50, bone tissue is created at a substantial velocity. Until the end of the simulation, bone continues to be formed but at a slower rate, filling a large part of the total domain.

Increasing the load from 1 MPa to 2 MPa leads to an increase of 11.85844531% in bone formation at the end of the simulation. However, the bone formation is not superior for the 2 MPa simulation from the beginning. In fact, in the first days, the superior load corresponds to a superior mechanical stimulus, surpassing the interval corresponding to bone formation. Later on, this higher mechanical stimulus becomes beneficial. Analyzing in greater detail, the formation of cartilage is vastly superior when 2 MPa are applied, especially between days 17 and 22, around the time when it reaches its maximum value (compare green areas of Figure 2 (a) and Figure 2 (b)). Afterwards, the rate of cartilage formation suffers an abrupt decrease which occurs simultaneously with the expeditious increase of bone formation, which means that the newly formed cartilage is under the influence of the conditions specified for endochondral ossification to occur, leading to cartilage calcification and, consequently, to its replacement by bone.

When comparing the results concerning the percentage of tissue formation for the 1 MPa loading condition with the computational results obtained in [17] for a permeability optimized microstructure an acceptable agreement is encountered. Also, the prediction of bone formation by [21], for a 30% porous scaffold in similar conditions, seems to be in accordance in terms of timing and magnitude with the current work results.

Figure 3 displays the evolution of the effective normal (C_{xx}, C_{yy}, C_{zz}) and shear (G_{xy}, G_{yz}, G_{xz}) stiffness components of the stiffness tensor. The curves represent the decay of the mechanical properties of the system as the biomaterial is hydrolyzed, followed by an increase due to the contribution of the newly formed tissues. Due to the symmetry of the microarchitecture, the initial values are the same in every direction. As time goes by, due the randomness of the degradation model, the components start to deviate a little. Nevertheless, they remain somewhat close, specially the values referring to the mechanical properties in the y and z directions evidencing that the tissue regeneration occurs in an almost symmetrical manner, as a consequence of the symmetry of the initial microarchitecture.

In [22], the evolution of the stiffness components of scaffold-tissues systems was also analyzed. The considered scaffolds were constituted by PCL, a polyester with a similar Young's modulus to that of PLGA. Simulations with three different scaffolds were performed, with ranging porosity values from 75-85% and with different pore distributions. There is a concordance regarding the shape of the evolution lines, especially with the more symmetric microarchitecture tried by Sanz-Herrera et al. [22]. There are discrepancies regarding the values, explained by the different porosity values of the scaffolds used on both studies. As the initial values of the stiffness constants for a scaffold with 35% porosity are superior, the descent due to the degradation of the biomaterial is steepest. Besides that, different bone Young's moduli are used, in fact, in [22] the remodeling of the non-mature bone into mature one was considered, whereas in this work it was not.

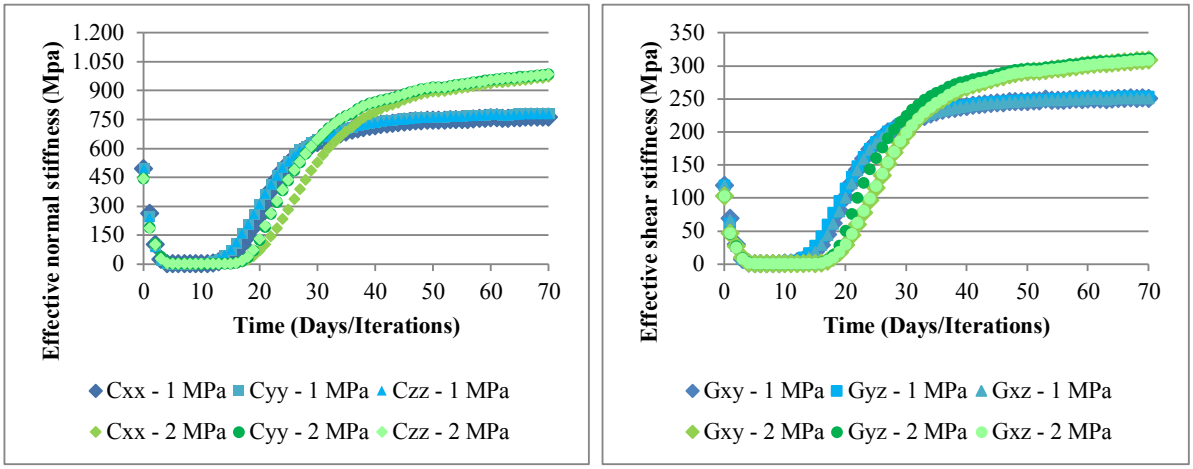

Fig. 3. Evolution of the (a) effective normal stiffness and (b) effective shear stiffness of the scaffold-tissues systems.

Regarding the effective permeability coefficients, P_x, P_y and P_z, their evolution through stimulation time is illustrated in Figure 4. In the first days, an increase is observed as the polymer matrix is degraded. After that, the permeability constants begin to decrease their values as new tissues are generated. The formation of fibrous tissue and cartilage would further increase the permeability of the system, however since bone is considered to have a much lower permeability (Table 1.) and considering that all tissues begin to form at an approximate time, the positive effect of cartilage and fibrous tissue formation is almost imperceptible. In the simulation of 2 MPa, as there is a greater amount of cartilage and fibrous tissue to be formed comparing to the quantity of bone generated, in the first 20 days, there is a further increase prior to the decay of the permeability constants.

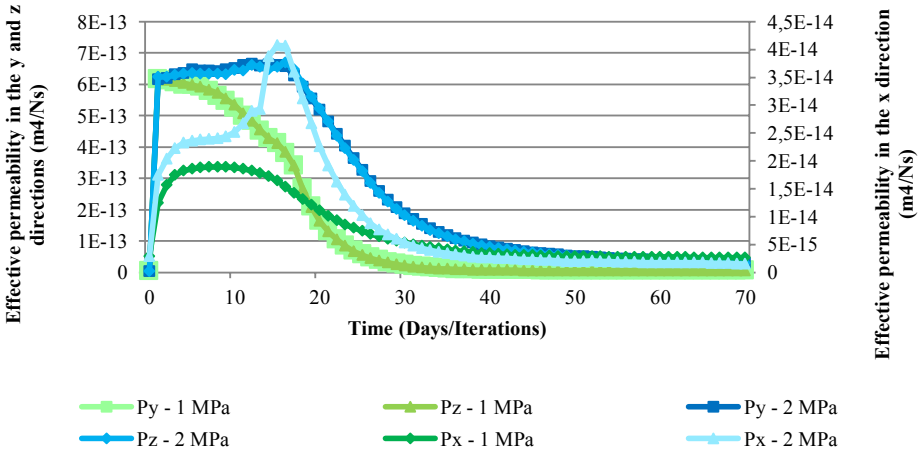

Fig. 4. Evolution of the effective permeability for the scaffold-tissues systems.

4. Conclusions

The implemented computational model is a solid starting point to develop a tool capable of providing new insights about the design and behavior of biodegradable artificial tissue substitutes. The degradation of the polymer matrix was modeled as the result of hydrolysis enhanced by an autocatalystic process and the obtained predictions are in a

good agreement with other computational and experimental data. The tissue formation was also adequately assessed through the implementation of a mechano-regulated model, based on cell differentiation and growth.

The most relevant findings are that under normal loading conditions, increasing the scaffold porosity resulted in higher percentages of bone formation while for higher load magnitudes, the porosity must be balanced with mechanical stability. Despite the accuracy of the model, some of the following improvements are in order. Since a possible strategy to enhance and accelerate the process of bone regeneration is the incorporation of growth factors in the porous matrices [23], it is desirable to consider their impact. Besides growth factors dependence, bone formation is highly susceptible to vascularization, so a more refined consideration of the vascularization effect on osteogenic pathways should be pursued.

Acknowledgement

This work was funded by Fundação para a Ciência e Tecnologia through the IDMEC, under LAETA, project UID/EMS/50022/2013 and through the PhD grant SFRH/BD/80458/2011.

References

[1] Y. Liu, J. Lim, S.-H Teoh, Review: Development of clinically relevant scaffolds for vascularised bone tissue engineering, Biotechnology advances, 31(5) (2013) 688– 705.
[2] Q. Fu, E. Saiz, M. N. Rahaman, A. P. Tomsia, Bioactive glass scaffolds for bone tissue engineering: state of the art and future perspectives, Materials Science and Engineering: C, 31(7) (2011) 1245–1256.
[3] S.J. Hollister, C.Y. Lin, Computational design of tissue engineering scaffold, Comput Methods Appl Mech Eng, 196 (2007) 31–2.
[4] M.R. Dias, J.M. Guedes, C.L. Flanagan, S.J. Hollister, P.R. Fernandes, Optimization of scaffold design for bone tissue engineering: A computational and experimental study, Medical engineering & physics, 36(4) (2014) 448–457.
[5] M. Castilho, M. Dias, U. Gbureck, J. Groll, P. Fernandes, I. Pires, B. Gouveia, J. Rodrigues, E. Vorndran, Fabrication of computationally designed scaffolds by low temperature 3D printing. Biofabrication 5 (2013) 035012.
[6] G. Chao, S. Xiaobo, C. Chenglin, D. Yinsheng, P. Yuepu, L. Pinghua, A cellular automaton simulation of the degradation of porous polylactide scaffold: I. Effect of porosity, Materials Science and Engineering: C, 29(6) (2009) 1950–1958.
[7] A. Göpferich, R. Langer, Modeling of polymer erosion, Macromolecules, 26(16) (1993) 4105–4112.
[8] A. Göpferich, Polymer bulk erosion, Macromolecules, 30(9) (1997) 2598–2604.
[9] Y. Mohammadi, E. Jabbari, Monte carlo simulation of degradation of porous poly (lactide) scaffolds, 1. Macromolecular theory and simulations, 15(9) (2006) 643–653.
[10] Y. Chen, S. Zhou, Q. Li, Mathematical modeling of degradation for bulkerosive polymers: applications in tissue engineering scaffolds and drug delivery systems, Acta biomaterialia, 7(3) (2011a) 1140–1149.
[11] J. Sanz-Herrera, J. Garcia-Aznar, M. Doblare, A mathematical approach for tissue regeneration inside a specific type of scaffold, Biomech Model Mechanobiol 7 (2007) 355–66
[12] T. Adachi, Y. Osako, M. Tanaka, M. Hojo, S.J. Hollister, Framework for optimal design of porous scaffold microstructure by computational simulation of bone regeneration, Biomaterials 27 (2006) 3964–3972
[13] P. G. Coelho, S.J. Hollister, C. L. Flanagan, P. R. Fernandes, Bioresorbable scaffolds for bone tissue engineering: Optimal design, fabrication, mechanical testing and scale-size effects analysis, Medical Engineering and Physics 37 (2015) 287–296
[14] M. Gómez-Benito, J. Garcia-Aznar, J. Kuiper, M. Doblaré, Influence of fracture gap size on the pattern of long bone healing: a computational study, Journal of theoretical biology, 235(1) (2005) 105–119.
[15] J. Guedes, N. Kikuchi, Preprocessing and postprocessing for materials based on the homogenization method with adaptive finite element methods, Computer methods in applied mechanics and engineering, 83(2) (1990) 143–198.
[16] M. Dias, P. Fernandes, J. Guedes, S. Hollister, Permeability analysis of scaffolds for bone tissue engineering, Journal of biomechanics, 45(6) (2012) 938–944.
[17] Y. Chen, S. Zhou, Q. Li, Microstructure design of biodegradable scaffold and its effect on tissue regeneration, Biomaterials, 32(22) (2011b) 5003–5014.
[18] M. Pilia, T. Guda, M. Appleford, Development of composite scaffolds for load-bearing segmental bone defects, BioMed research international, 2013.
[19] X. S. Wu, N. Wang, Synthesis, characterization, biodegradation, and drug delivery application of biodegradable lactic/glycolic acid polymers. Part II: Biodegradation, Journal of Biomaterials Science, Polymer Edition, 12(1) (2001) 21–34.
[20] S. H. Oh, S. G. Kang, J. H. Lee, Degradation behavior of hydrophilized PLGA scaffolds prepared by melt-molding particulate-leaching method: comparison with control hydrophobic one, Journal of Materials Science: Materials in Medicine, 17(2) (2006) 131–137.
[21] D. P. Byrne, D. Lacroix, J. A. Planell, D. J. Kelly, P. J. Prendergast, Simulation of tissue differentiation in a scaffold as a function of porosity, young's modulus and dissolution rate: application of mechanobiological models in tissue engineering, Biomaterials, 28(36) (2007) 5544–5554.
[22] J. Sanz-Herrera, M. Doblaré, J. GarcíaAznar, Scaffold microarchitecture determines internal bone directional growth structure: a numerical study, Journal of biomechanics, 43(13) (2010) 2480–2486.
[23] X. Wang, J. Nyman, X. Dong, H. Leng, M. Reyes, Fundamental biomechanics in bone tissue engineering, Synthesis Lectures on Tissue Engineering, 2(1) (2010) 1– 225.